

A Histogram - Based Algorithm for Semiautomated Three-Dimensional Craniofacial Modeling

by Richard A. Levy, M.D.

Department of Radiology

University of Michigan Hospitals

Introduction: Volume averaging artifacts in medical imaging result from voxel occupancy by more than one tissue type and, with anisotropic voxels, may be decreased by changing the imaging plane orientation relative to the target tissue and/or by decreasing slice thickness.¹

In craniofacial CT imaging, volume averaging artifact becomes significant in areas of thin bone such as the orbital walls and auditory ossicles. These regions are customarily imaged using multiple scan planes and the thinnest slices possible to reduce such artifacts. In three-dimensional craniofacial imaging, these same parameters may be controlled to reduce partial volume averaging, but areas of bone "drop-out" (also called pseudoforamina) are commonly present secondary to a paradoxical inability to lower thresholds without including unwanted background tissues. At present, the optimal solution to this problem is achieved by manually (and often painstakingly) drawing a region of interest around tissues presumed to contain volume averaged target density voxels and lowering thresholds to include these voxels in the 3D reconstruction, one CT slice at a time.

Recently, anatomic modeling technologies have demonstrated the feasibility of assembling particulate hydroxyapatite (synthetic bone) into detailed craniofacial models of high anatomic accuracy, theoretically suitable for in vivo implantation (work in progress with the Department of Mechanical Engineering, University of Texas at Austin.) These modeling systems, such as stereolithography and selective laser sintering, operate as do 3D imaging workstations, using thresholds to

include/exclude pixels from CT data sets in the modeling process. However, the user interactive capabilities of such technologies may be limited such that manual tracing of regions of volume averaged thin bone is not possible. Drop-out artifacts in models so generated would be potentially larger than on corresponding 3D images where user input could reduce these artifacts. To circumvent this inability to manually correct volume averaging artifacts on anatomic modeling systems, and to relieve the intensive operator input required to otherwise achieve this goal on 3D imaging software, a histogram-based algorithm for semiautomated three-dimensional craniofacial modeling was developed.

Materials CT data sets from 5 axially and coronally-scanned embryologic
and Methods: craniofacial specimens (aged 18 to 33 weeks) were used to generate one-dimensional histograms of entire imaging volumes. Histograms were constructed with the y-axis representing frequency and the x-axis representing CT number in Hounsfield units. Superimposition of histograms from corresponding orthogonal CT data sets from each case tested the hypothesis that voxel anisotropy produces divergence of corresponding segments of the histograms over ranges of Hounsfield density in which partial volume averaging occurs. These regions of volume averaging were predicted from prior phantom trials based upon 1) divergence of the histograms and/or presence of an asymmetric "tail" in an otherwise symmetric tissue distribution 2) very small numbers of pixels compared to the large populations of bone, soft tissue/water and air and 3) locations intermediate in Hounsfield density to the standard tissue distributions (Figures 1a and 1b). Thresholds based on these assumptions and on prior experimentation with this CT phantom applied to the histograms were compared with CT image-derived operator-selected thresholds. Most bone density pixels were identified using a simple formula obtained from prior phantom trials, $T=0.16|D-D_{ol}+D_o$, where

T=threshold, D=mean of bone pixel distribution, and D_0 =mean of soft tissue distribution.² In cases in which volume averaging was predicted from the histograms, the corresponding threshold ranges were expanded and contracted to assess the "uniqueness" of the predicted threshold ranges. All 3-dimensional CT images were generated using a volumetric rendering algorithm. Pathologic correlation consisting of craniofacial specimen photographs was available in some cases.

Results: Only in 1/5 cases (the 33 week specimen) could bone, soft tissue/water and air populations all be identified from the histograms. In the remaining 4/5 cases, only bone and air "peaks" were identified, with soft tissue/water voxels distributed more broadly over less well-defined Hounsfield density ranges. The ability to set thresholds was related to the ease with which the means of these tissue populations could be identified.

In 3/5 cases, inspection of the histograms permitted identification of discrete ranges of Hounsfield density over which partial volume averaging occurred. As anticipated, inclusion of non-osseous volume averaged voxels in the 3D reconstructions also occurred, principally at air-tissue interfaces such as the skin surface and surface of mucous membranes (Figure 2). In all cases in which volume averaging was predicted from the histograms, expansion of the threshold ranges beyond those predicted yielded inclusion of non-osseous tissue in the 3D reconstructions. In 2/3 of these cases, contraction of the threshold ranges caused loss of bone-density voxels from anatomic regions where bone was observed to fill-in using the predicted threshold ranges (Figure 2). In the remaining case, pathologic verification was not available.

Discussion: While volume averaging artifacts may be tolerated in 3D craniofacial imaging, they become more critical in craniofacial modeling, especially with the expectation that biosynthetic (e.g., hydroxyapatite) implants will promote osteoneogenesis.^{3,4} Tolerance of "drop-out" artifacts in a craniofacial implant will depend on the size and location of such defects.

The histogram-based thresholding algorithm presented in this essay proposes to diminish volume averaging artifact as well as the operator time involved in the generation of craniofacial implants from CT data. At present, the rate limiting factor is the time required for data transfer from the CT console to the generation of histograms.

Optimally, this process results in a single threshold on the order of 150 HU, as well as a range of lower CT density, e.g., -100 to -400 HU (Figure 2). For the purpose of anatomic modeling, undesired volume averaged tissues such as the skin surface can be dissected from the implant.

A potential pitfall to this method is its dependency upon the presence of well-defined bone, water/soft tissue and air-density histogram populations to permit the initial selection of thresholds. It is likely that the small specimen size used in this experiment contributed to the absence of definable water/soft tissue peaks in most cases, especially since the expected tissue distributions were achieved only with the largest (33 week) specimen. While the utilization of such small craniofacial specimens has the advantage of eliminating (potential positionally-dependent) beam hardening artifacts, it is anticipated that further trials with this method will occur with postnatal and adult subjects.

Another potential pitfall awaiting evaluation in clinical trials of this algorithm arises from the fact that, in the present experiment, the imaging volume encompassing

the entire craniofacial specimen was included in both the paired axial and coronal data sets. In the clinical setting, this may not be possible, making identification of volume-averaged voxels more challenging.

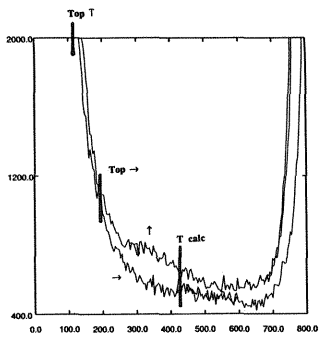
References

1. Levy RA, Edwards WT, Meyer JR, Rosenbaum AE. Facial trauma and 3-D reconstructive imaging: insufficiencies and correctives. *AJNR* 1992;13:885-892.
2. Levy RA. Semiautomated three-dimensional craniofacial imaging and modeling. *Investigative Radiology* 1994;29(2):150-155.
3. Damien CJ, Parsons JR, Benedict JJ, Weisman DS. Investigation of a hydroxy-apatite and calcium sulfate composite supplemented with an osteoinductive factor. *J Biomed Mater Res* 1990 24(6):639-654.
4. Levy RA. U.S. Patent Pending, "Three-dimensional model generation from multiple tomographic scan planes."

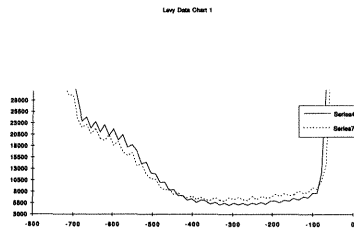
Legend to Figures

Figure 1a Superimposition of one dimensional histograms of a polyvinylchloride phantom scanned in water from the axial (\rightarrow) and coronal (\uparrow) planes. The y-axis indicates frequency. T_{calc} = average Hounsfield density of the means of the water and phantom pixel/voxel distributions. $Top \rightarrow$, $Top \uparrow$ = operator-selected thresholds for 3D reconstructions generated from axial and coronal data, respectively. Note gradual upslope ("tail") as well as slight divergence of the histograms in the intervals defined by T_{calc} and Top , with the histogram generated from coronal data (\uparrow) having the larger number of pixels. The intervals defined by T_{calc} and Top were demonstrated to contain volume averaged voxels in submillimeter structures in the phantom that "filled-in" using the lower thresholds, Top . These structures were better visualized on 3D imaging using the axial (\rightarrow) data at a numerically larger Top , consistent with less volume averaging in the axial (\rightarrow) 2D CT data set.

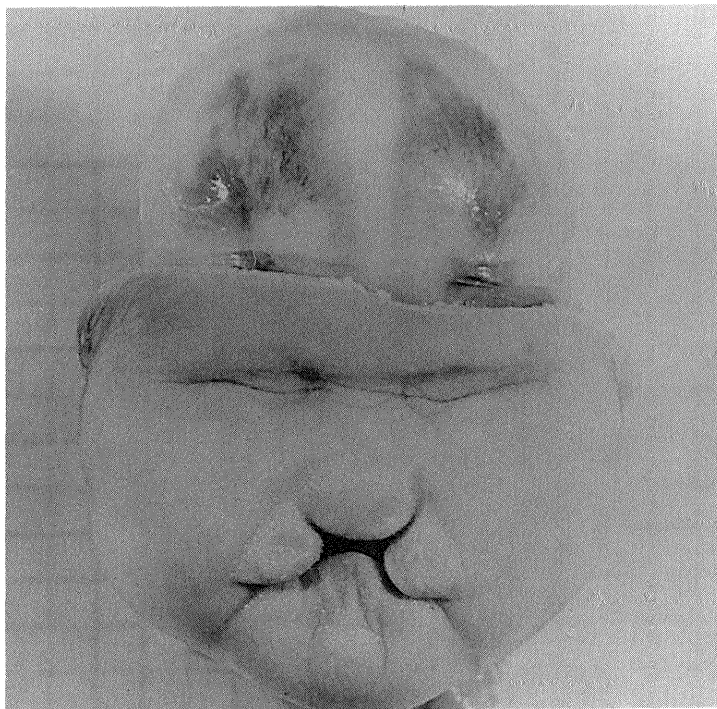
- Figure 1b Superimposed one dimensional histograms generated from axial and coronal 2D CT data sets of a 33 week craniofacial specimen with holoprosencephaly. Note "inversion" of the histograms between -100 and -400 HU, with the coronal data set having the greater number of pixels/voxels. Volume averaged voxels would be expected to appear on 3D reconstruction using an additional threshold of -100 to -400 HU, with greater "fill-in" on the 3D reconstruction generated from coronal data.
- Figure 2a Photograph of the 33 week holoprosencephalic specimen. Note intact frontal bones.
- Figures 2b,2c 3D reconstructions from axial (2b) and coronal (2c) data using operator-selected thresholds of 183 and 186, respectively. Note better "fill-in" of frontal bone voxels using axial data.
- Figure 2d 3D reconstruction from coronal data using the histogram-derived threshold of 130.
- Figure 2e 3D reconstruction from coronal data using the combined thresholds of 130 and -100 to -400. Note "fill-in" of frontal bone voxels(*) as well as other volume averaged tissues such as the skin surface (arrow) and mucous membrane surface (double arrows).
- Figure 2f Same as in 2e but using axial data, illustrating inclusion of skin surface and mucous membrane volume averaged voxels to a similar extent as with the coronal data set. This indicates that the region of histogram divergence between -100 to -400 HU in Figure 1b where the coronal data set contains a greater number of voxels corresponds to volume averaged frontal bone voxels in the coronal data set. Voxels between -100 to -400 HU are color coded in grey.
- Figure 2g Same as in 2e but with lower threshold expanded to -100 to -500 HU. Note appearance of background shroud (arrow). Voxels from -100 to -500 HU are color-coded in grey.
- Figure 2h Same as in 2e but with lower threshold contracted to -150 to -250. Note drop-out of bone density voxels from the frontal bones (arrow).
- Figure 2i Same as in 2e but with threshold of -100. Note fill-in of soft tissue between skin surface and bone, and drop-out of bone voxels from the frontal bones (*).



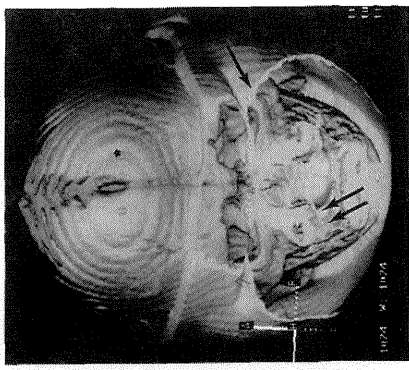
1a



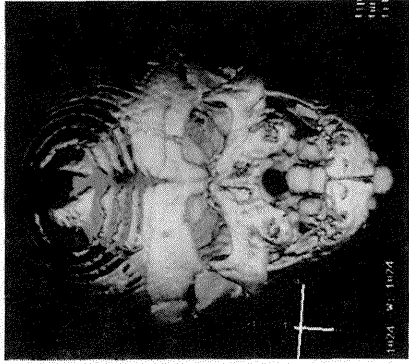
1b



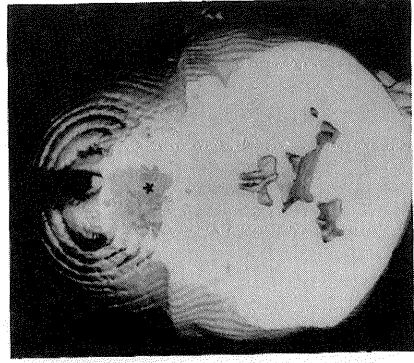
2a



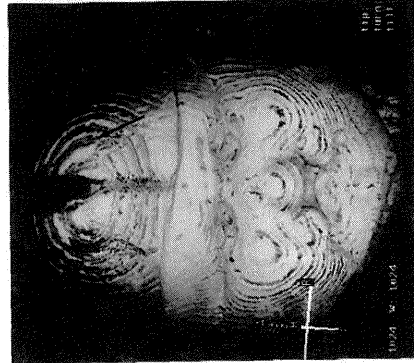
2e



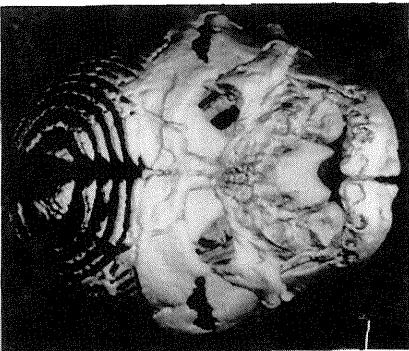
2d



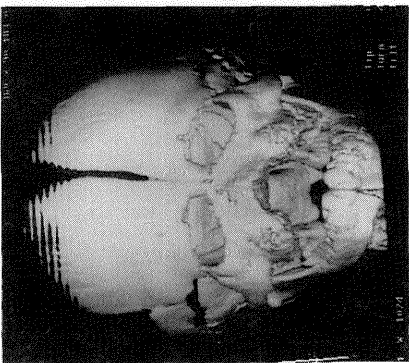
2i



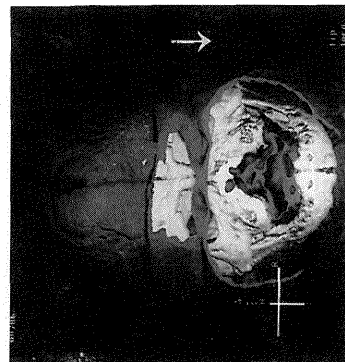
2h



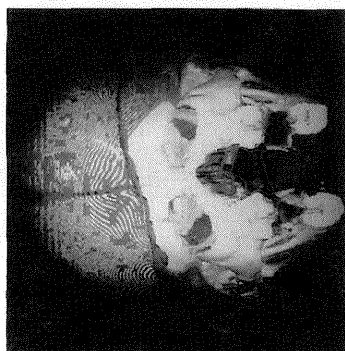
2c



2b



2g



2f